AGU PUBLICATIONS

Geophysical Research Letters

RESEARCH LETTER
10.1002/2017GL074111

Key Points:
- Cyclostationary empirical orthogonal functions are used to analyze the effects of climate oscillations on wildland fire potential
- The modulated annual cycle is primarily associated with variations in wildland fire potential in the western U.S. and Florida
- Effects of El Niño and La Niña are widespread, with the largest changes relative to the mean occurring in the northwest and southeast

Supporting Information:
- Supporting Information S1

Correspondence to:
P. E. Hamlington,
peh@colorado.edu

Citation:
Mason, S. A., P. E. Hamlington, B. D. Hamlington, W. Matt Jolly, and C. M. Hoffman (2017), Effects of climate oscillations on wildland fire potential in the continental United States, *Geophys. Res. Lett.*, *44*, 7002–7010, doi:10.1002/2017GL074111.

Received 11 MAY 2017
Accepted 22 JUN 2017
Accepted article online 27 JUN 2017
Published online 12 JUL 2017

Effects of climate oscillations on wildland fire potential in the continental United States

Shelby A. Mason[1], Peter E. Hamlington[1], Benjamin D. Hamlington[2], W. Matt Jolly[3], and Chad M. Hoffman[4]

[1]Department of Mechanical Engineering, University of Colorado, Boulder, Colorado, USA, [2]Department of Ocean, Earth and Atmospheric Sciences, Old Dominion University, Norfolk, Virginia, USA, [3]U.S. Forest Service, Rocky Mountain Research Station, Fire Sciences Laboratory, Missoula, Montana, USA, [4]Department of Forest and Rangeland Stewardship, Colorado State University, Fort Collins, Colorado, USA

Abstract The effects of climate oscillations on spatial and temporal variations in wildland fire potential in the continental U.S. are examined from 1979 to 2015 using cyclostationary empirical orthogonal functions (CSEOFs). The CSEOF analysis isolates effects associated with the modulated annual cycle and the El Niño–Southern Oscillation (ENSO). The results show that, in early summer, wildland fire potential is reduced in the southwest during El Niño but is increased in the northwest, with opposite trends for La Niña. In late summer, El Niño is associated with increased wildland fire potential in the southwest. Relative to the mean, the largest impacts of ENSO are observed in the northwest and southeast. Climate impacts on fire potential due to ENSO are found to be most closely associated with variations in relative humidity. The connections established here between fire potential and climate oscillations could result in improved wildland fire risk assessment and resource allocation.

1. Introduction

It is anticipated that, over the coming decades, climate change will contribute to increased wildland fire activity, particularly in the western U.S. [*Westerling et al.*, 2006; *McKenzie et al.*, 2004]. Due to the negative environmental and human impacts resulting from such an increase, fire management agencies are now using seasonal climate forecasts for planning, long-range fire behavior prediction, resource allocation, and risk assessment [*Garfin and Morehouse*, 2001]. These forecasts depend heavily, however, on predictions of internal climate oscillations, including the modulated annual cycle (MAC) [*Wu et al.*, 2008], which describes the interannual variability in the seasonal cycle, and the El Niño–Southern Oscillation (ENSO) [*Ropelewski and Halpert*, 1986; *Ropelewski and Halpert*, 1987]. The MAC is associated with variations in the strength of the seasonal cycle and is due to interannual phenomena such as changes in solar intensity. These and other oscillations influence the climate in a variety of ways, resulting in subsequent impacts on wildland fire risk and potential [*Gershunov and Barnett*, 1998; *Barbero et al.*, 2015; *Morgan et al.*, 2008]. The primary objective of the present study is to better understand impacts of the MAC and ENSO on fire potential in the continental U.S.

Substantial prior research has addressed the connection between climate signals and wildland fires. For example, linkages have been made between wildland fires and the combined effects of ENSO and the Pacific Decadal Oscillation [*Crimmins*, 2010; *Hessl et al.*, 2004; *Heyerdahl et al.*, 2008]. The effects of longer-term climate change have also been examined [*Brown et al.*, 2004; *Trouet et al.*, 2006; *Fauria et al.*, 2010; *Flannigan et al.*, 2009; *Jolly et al.*, 2015; *Williams and Abatzoglou*, 2016]. In the U.S., *Beckage et al.* [2003] found that ENSO affects wildland fires in the Florida Everglades by changing the amount of dry-season rainfall and by influencing the frequency of lightning strikes. *Brenner* [1991] also analyzed ENSO effects in Florida, finding a relationship between acres burned and anomalous sea surface temperature and sea level pressure in the central and eastern Pacific. In the southwest U.S., *Swetnam and Betancourt* [1990] found that wildland fires were larger and more frequent in summers immediately following the dry phase associated with La Niña winters (although the same trends may not be present at fuel-limited lower elevations). Similarly, *Brown et al.* [2008] found that there were more wildland fires in Utah during La Niña events and fewer fires during El Niño events. Paleoecological data and fire-scarred tree ring reconstructions generally support the observation that climate variability is a dominant factor affecting large wildfires in the western U.S. [*McKenzie et al.*, 2004; *Kitzberger et al.*, 2007].

Despite this prior work, there is still considerable uncertainty regarding the specific impacts of different climate oscillations on wildland fire potential for the entire continental U.S. Although previous studies have related the MAC to wind resource variability [*Hamlington et al.*, 2015] and surface air temperature [*Qian et al.*, 2011], both of which are relevant to wildland fire potential, little understanding exists of the connection between the MAC and wildland fires. It is also difficult to separate the specific impacts of simultaneously occurring climate oscillations, each with different phases and periods. Moreover, many previous studies of climate oscillations, and ENSO in particular, have been based on focused regional observational campaigns that are unable to provide simultaneous information about climate effects on wildland fire potential for the entire continental U.S.

In order to more effectively determine the spatial and temporal variability of wildland fire potential due to the MAC and ENSO in the continental U.S., cyclostationary empirical orthogonal functions (CSEOFs) [*Kim et al.*, 2015] are used here to analyze the U.S. Burning Index (BI). The BI quantifies fire danger related to potential flame length and depends on environmental factors such as temperature, precipitation, relative humidity, and wind speed. When combined with site descriptions, these factors control the moisture content of wildland fuels, which strongly affects fire spread rate and the energy released by burning [*Bradshaw et al.*, 1984; *Flannigan et al.*, 2015]. Although the BI is positively associated with wildland fire occurrence [*Preisler et al.*, 2004] and the seasonal BI is positively associated with area burned [*Abatzoglous and Kolden*, 2013], the BI is strictly a measure of anticipated wildland fire potential and the difficulty of fire containment. The BI is also largely based on atmospheric conditions and does not account for fuel abundance or accumulation. The BI has been used previously to relate climate effects and fire season length [*Jolly et al.*, 2015], and it is used here to determine specific impacts of the MAC and ENSO on wildland fire potential.

2. Data and Methods

The present CSEOF analysis is based on monthly-averaged BI values calculated for the continental U.S. using data from the National Centers for Environmental Prediction North American Regional Reanalysis (NARR) weather data set, which covers the time period from 1979 to 2015 [*Mesinger et al.*, 2006]. This data set provides wind speed, relative humidity, temperature, and precipitation 8 times per day with 0.3° spatial resolution. Using these data, spatial maps of the BI are calculated and then averaged monthly to obtain the analysis data set. Although this approach precludes examination of diurnal variations in the BI, monthly-averaged data are sufficient for examining longer term interannual climate oscillations, which are the focus of this study.

2.1. Burning Index Calculation

Four types of data are used to calculate the BI: (i) static site descriptions, (ii) daily observations, (iii) 24 h observations, and (iv) carry-over values [*Bradshaw et al.*, 1984]. Site descriptions include the fuel model, slope class, live fuel types, climate class, latitude, and annual average precipitation for the site. The temperature, relative humidity, cloud cover, and wind speed measured at 1300 LST are input for the daily observations. The 24 h observations include maxima and minima of temperature and relative humidity, as well as precipitation duration. Carry-over values of heavy dead fuel moistures from the previous 7 days are also input to the system. Daily means and extremes of temperature and humidity, daily precipitation duration, and maximum daily wind speed are derived from the NARR data set to provide both daily and 24 h observations for all calculations. Fuel model G is used at all locations to provide a standard fire danger metric across the study area [*Jolly et al.*, 2015]. Carry-over values are maintained internally for all daily calculations. All of these inputs are used to calculate the fuel moisture for 1, 10, 100, and 1000 h dead down woody time lag fuel classes [*Fosberg et al.*, 1970]. These general classes are commonly used in fire management as descriptors of potential fire behavior and are based on the rates of drying associated with fuel components of various sizes. The resulting fuel moistures are used to calculate the BI, which is linearly related to the potential flame length at the head of the fire and represents the difficulty of fire containment [*Bradshaw et al.*, 1984].

2.2. Cyclostationary Empirical Orthogonal Function Analysis

Using time-resolved spatial maps of BI with monthly resolution, a CSEOF analysis is performed in order to extract the variability associated with the MAC and ENSO. As described in previous work [*Hamlington et al.*, 2011; *Hamlington et al.*, 2015], the CSEOF method decomposes space-time data into a series of modes

consisting of a spatial component (known hereafter as the loading vector (LV)) and a corresponding temporal component (known as the principal component time series (PCTS)). The LVs represent spatial patterns of variability of the BI, and the PCTS represents temporal variations of these patterns. Complete spatial-temporal CSEOF modes are obtained by multiplying the LVs and the nondimensional PCTS. Substantial additional detail on the CSEOF method is provided in *Kim et al.* [2015] and is also described at length in *Hamlington et al.* [2011].

The primary difference between the CSEOF technique and traditional eigenvalue analyses is that CSEOFs have time-dependent LVs that are constrained to be periodic with a set nested period. The nested period is selected based on physical understanding of the data being analyzed. In this way, the LVs are spatial maps that capture the temporal evolution of the BI within the specified nested period. The corresponding PCTS explains the amplitude of the LVs through time. As an example, when studying the annual cycle in monthly data, a 1 year nested period would be selected. Each LV would consist of 12 maps (one for each month) describing the 1 year oscillation, and the corresponding PCTS would show changes in strength of the annual cycle from year to year. CSEOFs avoid the assumption of stationarity in the decomposed spatial patterns and reduce the mixing of physical signals across several modes, as frequently occurs in more traditional analyses based on empirical orthogonal functions (EOFs). Although the formalism of the EOF approach is similar to the CSEOF method used herein, mode mixing in EOF approaches precludes an unambiguous identification of different climate signal effects on the BI. The ability to isolate specific cyclostationary climate signals from Earth system data is the primary advantage of the CSEOF method as compared to EOF methods.

The present study is the first to use CSEOFs for the analysis of climate oscillation impacts on wildland fires across the continental U.S. Previous studies, such as those by *Gedalof et al.* [2005], *Page et al.* [2008], and *Riaño et al.* [2007], have used EOF analysis when looking at area burned. However, the effects of climate oscillations are expected to vary both spatially and temporally, and understanding these variations requires the use of the CSEOF approach.

3. CSEOF Burning Index Analysis

Following previous CSEOF studies of climate oscillations [*Hamlington et al.*, 2011, *Hamlington et al.*, 2015], a 1 year nested period has been selected for the CSEOF analysis in order to target the variability associated with the MAC and ENSO. While this choice is obvious for studying the MAC, particularly given the 1 year periodicity of the annual cycle, the use of a 1 year nested period to capture ENSO variability is less obvious. Using a 1 year nested period, the ENSO-related LVs show the strengthening and weakening of ENSO effects that are known to occur over the course of a year, while the PCTS represents the occurrence of ENSO events. The analysis is specifically focused on anomalies in the BI, which are obtained by first removing mean and linear trends computed over the full data record at each spatial location. The magnitudes of the anomalies, representing departures from the mean BI at each location, are then captured by the CSEOF modes. Linear trend removal is necessary because, using the relatively short data record examined here, linear trends will be split across multiple CSEOF modes, thereby making the physical interpretation of each mode more difficult. Although the linear trend in the BI may be of interest for understanding the effects of climate change on the BI, connecting climate change to the BI using such a short data record is a challenge and not the focus of this paper.

CSEOF LVs are computed, providing a map for each of the 12 months within the 1 year nested period and then averaged over four seasons. These seasonal LVs and the corresponding PCTS for the first CSEOF mode are shown in Figure 1. This mode was found to represent 31% of the total observed variability in the BI anomaly. The four seasons, each spanning 3 months, are referred to here as late winter (January-February-March), early summer (April-May-June), late summer (July-August-September), and early winter (October-November-December). The PCTS in Figure 1 is strictly positive, which indicates that the physical period of the first-mode signal is fully described by the temporal variation of the LVs contained within the 1 year nested period [*Hamlington et al.*, 2011]. This allows the first mode to be identified as the MAC, which specifically indicates the strength of the seasonal cycle from year to year. As a result, when the MAC is at a maximum, there will be greater differences between summer and winter, as compared to years with a weaker MAC signal.

The LVs in Figure 1 show that, in the western U.S., BI anomalies are greatest (i.e., most positive) during both early and late summer, with the smallest (i.e., most negative) BI anomalies occurring during late winter. These results are consistent with annual temperature patterns, which have significant impacts on the BI calculation.

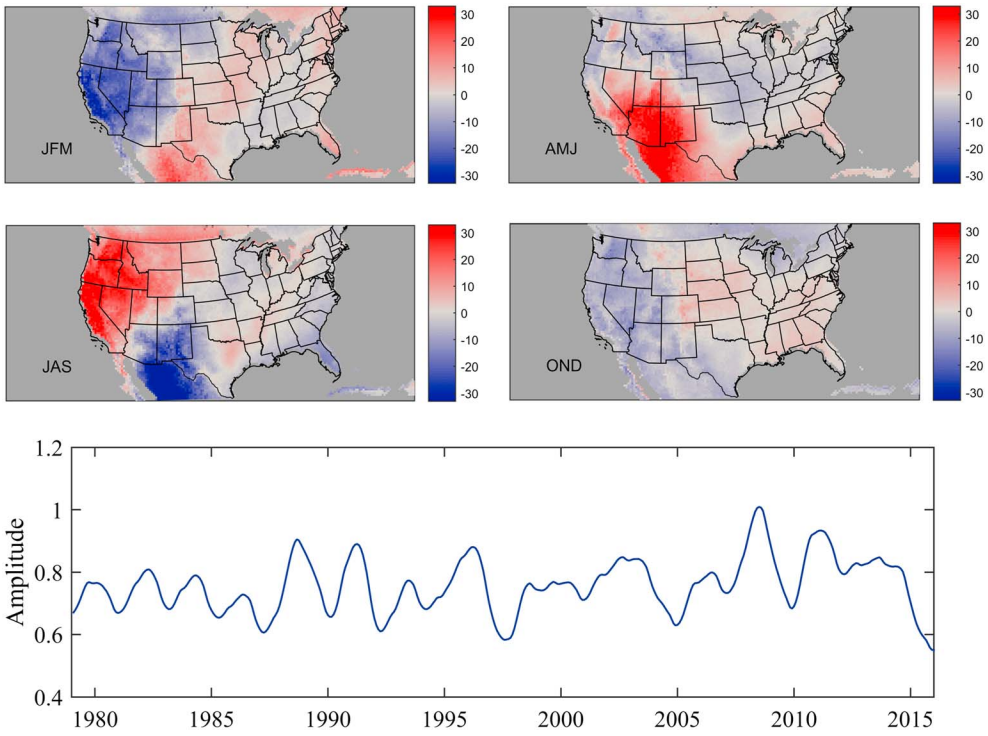

Figure 1. Mode 1 of the CSEOF decomposition, explaining the MAC, after removing the long-term trend for the BI so that the CSEOF analysis is performed on the BI anomaly. (top and middle rows) LVs for the dimensionless BI and the (bottom row) dimensionless PCTS, representing the interannual amplitude modulation of the annual cycle. The LVs are averaged monthly according to the labels to produce one map for each season.

There is also a significant increase in the BI anomaly in the southwest during early summer, and this increase expands to cover much of the western U.S. by late summer. More significantly for the purpose of understanding future BI variability, the PCTS reveals variations in the strength of this pattern from year to year. In particular, variations in the MAC from the mean approach 20%, indicating a strengthening of the seasonal cycle in some years (e.g., in 2008) and a weakening of the seasonal cycle in other years (e.g., in 2005). Since BI is a strictly positive quantity, it is likely that these variations are most directly associated with changes in the BI during the peak of fire season. There also appears to be a roughly 2 year period of variations due to the MAC.

In previous CSEOF studies of Earth system data, for example those focused on wind resource [*Hamlington et al.*, 2015] and sea level [*Hamlington et al.*, 2011] variability, the second CSEOF mode was found to be associated most closely with ENSO. The present results follow these prior studies, with the second mode closely matching the concurrent Multivariate ENSO Index (MEI) [*Wolter and Timlin*, 2011]. The MEI characterizes the intensity and phase of ENSO, where positive values represent El Niño events and negative values represent La Niña events. As noted previously [*Wolter and Timlin*, 2011], El Niño events represent larger positive values of the MEI as compared to the negative values for La Niña events.

In order to further improve the representation of ENSO impacts on the BI, the CSEOF modes are regressed onto the MEI using a technique described in *Hamlington et al.* [2011] and *Hamlington et al.* [2015]. This regression of the CSEOF modes reduces mode mixing and improves the representation of ENSO variability within a single mode, mitigating the challenges normally associated with a relatively short data record. The resulting regressed second CSEOF mode is shown along with the unregressed second mode PCTS and MEI in Figure 2. The unregressed second CSEOF mode explains 5% of the total variability in the BI anomaly, while the regressed mode likely explains roughly 10% of the total variability. Positive values of the PCTS in Figure 2 correspond to El Niño events and produce an increase in the BI when combined with a positive value in the LV maps and a decrease in the BI when combined with a negative value. The opposite is true for a La Niña event, which is associated with negative values of the PCTS and MEI. The bottom panel of Figure 2

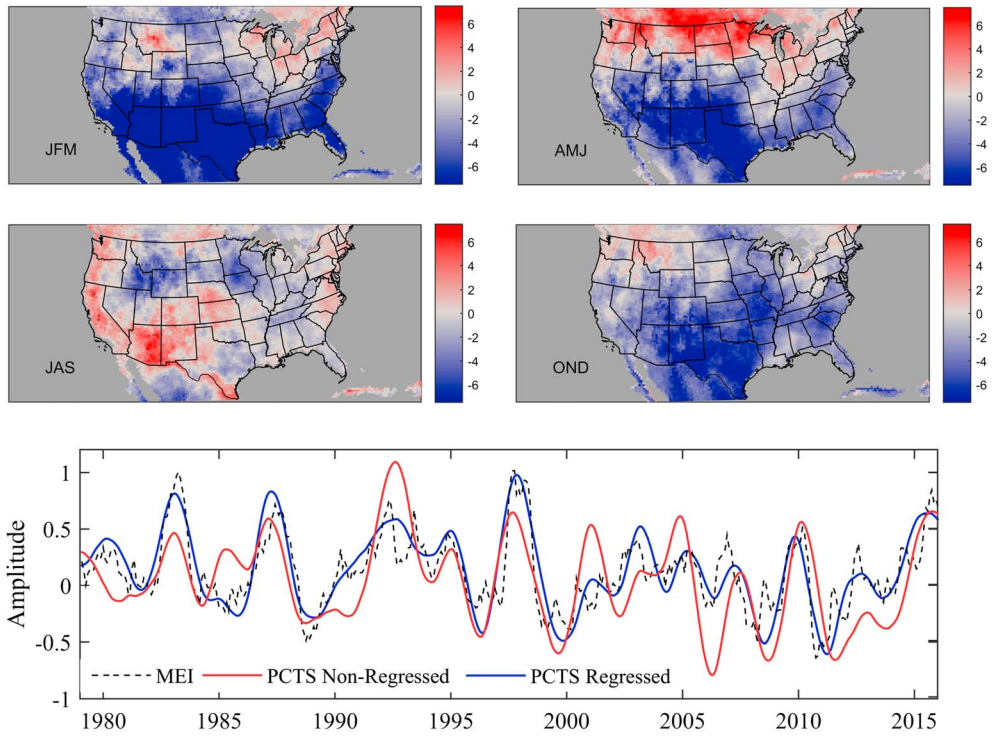

Figure 2. Regressed mode of the CSEOF decomposition, explaining the ENSO, after removing the long-term trend for the BI so that the CSEOF analysis is performed on the BI anomaly. (top and middle rows) LVs for the dimensionless BI and the (bottom row) dimensionless PCTS. The LVs are averaged monthly according to the labels to produce one map for each season. The Multivariate ENSO Index (MEI; black dashed) is plotted with the non-regressed PCTS (red) and the regressed PCTS (blue) to demonstrate the relationship between the mode and ENSO. The LV maps depict the positive phase of ENSO.

indicates that both the regressed and unregressed second mode PCTS are in relatively good agreement with the MEI, with correlations of 0.85 and 0.61, respectively.

The LVs in Figure 2 show that, during an El Niño (i.e., when the PCTS is positive), BI anomalies are negative in the southwest and positive in the northwest in early summer (note that such anomalies are obtained by multiplying the LVs by the corresponding value of the PCTS). This indicates greater wildfire potential in the northwest and lesser potential in the southwest during early summer in El Niño years. These general regional trends then shift in late summer, with positive BI anomalies in the southwest and negative anomalies in the northwest. The opposite effect is observed during La Niña events, where negative values of the PCTS are multiplied by the LVs to obtain positive BI anomalies in the southwest and negative anomalies in the northwest during early summer. This indicates greater wildfire potential in the southwest and reduced potential in the northwest during early summer in La Niña years. Once again, these regional effects switch during late summer, with negative BI anomalies in the southwest and positive anomalies in the northwest.

Furthermore, Figure 2 shows that much of the U.S. experiences negative BI anomalies during early winter of El Niño years, indicating reduced wildland fire potential. These negative anomalies are more pronounced in the southern half of the U.S. in late winter. There are similar negative anomalies in early summer in the southern U.S., which are paired with positive anomalies in the northern U.S., creating a north-south dividing line of zero BI anomaly. Opposite effects are observed during La Niña events, where the southern U.S. experiences positive BI anomalies in all but the late summer season. These anomalies, and the associated changes in wildland fire potential, are likely to have the greatest real-world impacts during early and late summer when wildland fire ignition is more common.

In order to further understand the possible range of influence resulting from MAC and ENSO variability, the maximum percentage increase and decrease in the BI relative to the long-term mean are shown in Figure 3 for both climate oscillations. These results are obtained by computing the largest and smallest values of the BI anomaly at each location for the first and second mode CSEOFs, and then normalizing by the mean value of

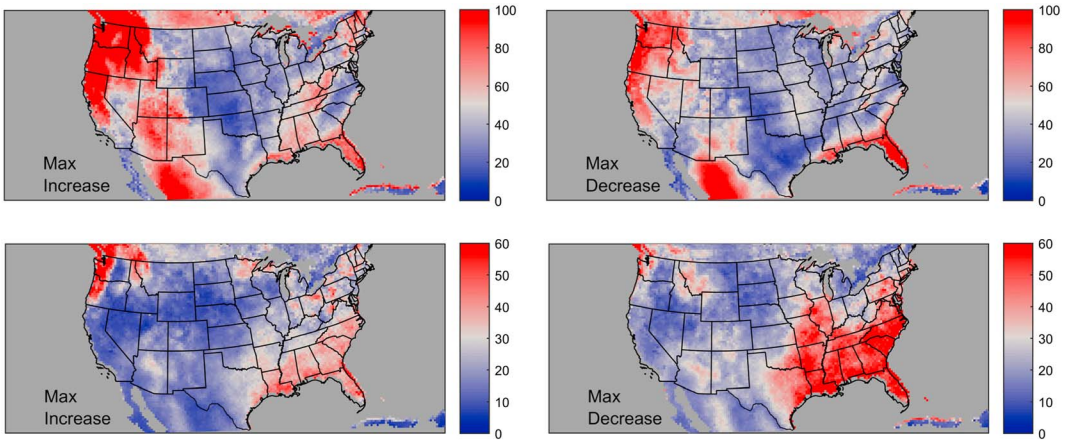

Figure 3. Maximum percentage (left column) increase and (right column) decrease in the BI anomaly relative to the long-term mean for the MAC (top row) and ENSO (bottom row), as given by the modes shown in Figures 1 and 2.

the BI at the same location. The largest increases and decreases in the BI due to the MAC occur in the western U.S. and in Florida, indicating that these are the regions most affected by changes in the strength of the seasonal cycle. By contrast, the greatest changes relative to the mean due to ENSO are observed in the northwest and southeast U.S. Comparison with Figure 2 indicates that ENSO-related increases in the northwest are associated with El Niño and increases in the southeast are most associated with La Niña. Changes relative to the mean are, overall, roughly twice as large for the MAC as compared to ENSO, and changes as large as 100% of the mean are seen for the MAC (that is, MAC-induced increases in the BI can be twice as large as the mean).

4. Discussion

In order to provide an explanation for the observed results, the same CSEOF regression analysis was performed on each of the variables from the NARR data set used in the calculation of the BI (i.e., temperature, precipitation, relative humidity, and wind speed). Each of these analysis results is shown in the supporting information. The results for the relative humidity and total precipitation were found to be most similar to the BI results in Figure 2. In particular, regional patterns and seasonal variability for the relative humidity closely match results for the BI in Figure 2. In this case, the second mode relative humidity PCTS closely matches the MEI.

These results suggest that the effects of ENSO on relative humidity and total precipitation have leading roles in determining ENSO-related spatial and temporal variability of the BI. This connection is not surprising; wildland fire potential is heavily dependent on fuel moisture and several prior studies have noted the impacts of variability in precipitation on wildland fires [*Flannigan et al.*, 2015; *Holden et al.*, 2007; *Ropelewski and Halpert*, 1986]. Increases in relative humidity and precipitation relative to the mean cause an increase in the fuel moisture content, which leads to a decrease in the BI. ENSO has also been shown to cause variability in the North American monsoon system [*Grantz et al.*, 2007], which heavily affects precipitation amounts in the southwest U.S. This relationship could explain the monthly reversal in the BI seen in the LVs, which is potentially caused by seasonal shifts in the North American monsoon and its accompanying precipitation.

In order to validate the trends obtained from the CSEOF analysis, observational statistics for acres burned in the areas of highest BI anomaly have been analyzed. Data for fire location and number of acres burned were obtained from the Monitoring Trends in Burn Severity (MTBS) burned area boundaries data set [*Eidenshink et al.*, 2007]. This data set spans the time period from 1984 to 2014 and leverages 30 m resolution images from the U.S. Geological Survey Landsat to map and characterize wildland fires. Acres burned is the preferred metric for evaluating BI results, since the BI represents the difficulty of containment of an already-ignited fire and so has no relation to fire occurrence itself. In this way, an ignited fire in an area with a relatively high BI will be more difficult to contain and therefore will be more likely to consume a larger number of acres.

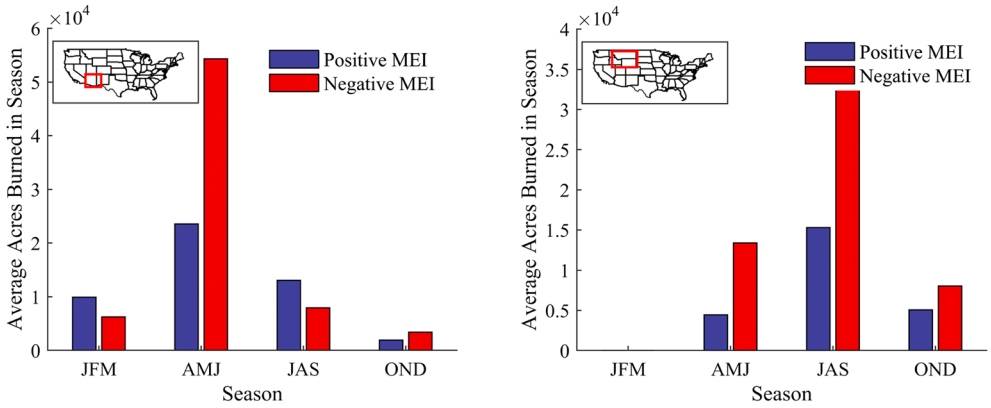

Figure 4. Statistics for acres burned at (left panel) southwest and (right panel) northwest locations, as indicated in the insets. Average acres burned for each season are shown for positive MEI months and negative MEI months.

Acres burned per fire in the southwest and northwest, averaged over each season, are shown in Figure 4 for both positive and negative MEI, corresponding to El Niño and La Niña conditions, respectively. Consistent with the BI results from the CSEOF analysis, there are smaller fires during early summer in the southwest for positive MEI years, as compared with negative MEI years. This relationship reverses in late summer, with positive MEI years producing comparatively larger fires. For the northwest in late summer, there are, on average, smaller fires during positive MEI years as compared with negative MEI years. This is again consistent with the CSEOF results, which predict low (high) BI values during positive (negative) MEI years. Higher BI values, such as those observed for the northwest in late summer during negative MEI years, indicate a more difficult to contain and therefore larger, fire per occurrence.

The impact of the MAC is also visible in Figure 4. Regardless of the phase of the MEI, there is a significant increase in acres burned in early summer for the southwest and in late summer in the northwest relative to the other seasons. This is consistent with the LVs shown in Figure 1. The increase seen in early (late) summer for the southwest (northwest) during La Niña conditions demonstrates the manner in which the MAC and ENSO can constructively combine to dramatically increase wildfire potential.

Once again, it is important to note that the BI does not take into account the ignition probability of wildland fires and thus has no direct relation to fire occurrence. Rather, the BI describes fire potential and difficulty of containment of an already-ignited fire. In this way, a location can have a high BI, but with no source of ignition, a fire will not occur. Similarly, a location can have a low BI yet still have multiple fires due to multiple ignition sources, although these fires will be relatively easier to contain.

5. Conclusions

Using CSEOFs, the effects of MAC and ENSO climate signals on the BI in the continental U.S. have been isolated. Burning index anomalies associated with the MAC follow annual temperature variations, with relative increases in the western U.S. during early and late summer. As a result of ENSO variability, the northwest and southwest U.S. experience a seasonal reversal in BI anomalies between early and late summer. During an El Niño phase in early summer, the southwest experiences a decrease from the mean BI and the northwest experiences an increase. These regional variabilities reverse as the year progresses into late summer. This seasonal shift is echoed in relative humidity and precipitation variations and is in good agreement with observational statistics of area burned.

Prediction of the BI based on the current strength and stage of a long-term climate cycle could result in improved wildland fire risk assessment and resource allocation. Given longer data records, the same CSEOF analysis presented here could also be used to separate decadal and multidecadal variability from long-term climate trends in the BI. It should be noted that while this study analyzes the BI, accurate and long-term fire ignition data could be used to further investigate fire occurrence. Further validation of the method and results presented herein are also necessary using additional data sets; the MTBS data set used

here considers only large fires where many acres are burned. Additionally, a more extensive and representative fuel model could be used to further research BI linkages to climate within specific ecoregions. Additional research is also required to more fully explain why variations in the BI occur due to the ENSO and MAC. Furthermore, while the present study utilizes a 1 year nested period, the same CSEOF analysis with a 2 year nested period could be used in future work to further examine the BI anomalies during the transition between El Niño and La Niña phases.

Acknowledgments
S.A.M. and P.E.H. acknowledge support from the Innovative Seed Grant Program at the University of Colorado, Boulder. P.E.H. also acknowledges support from SERDP under grant W912HQ-16-C-0026. NCEP Reanalysis data were provided by the NOAA/OAR/ESRL PSD, Boulder, Colorado, USA, from their Web site at http://www.esrl.noaa.gov/psd/.

References

Abatzoglous, J. T., and C. A. Kolden (2013), Relationships between climate and macroscale area burned in the western United States, *Int. J. Wildland Fire*, *22*(7):1003–1020.

Barbero, R., J. T. Abatzoglou, and T. J. Brown (2015), Seasonal reversal of the influence of El Niño–Southern Oscillation on very large wildfire occurrence in the interior western United States, *Geophys. Res. Lett.*, *42*, 3538–3545, doi:10.1002/2015GL063428.

Beckage, B., Platt, W. J., Slocum, M. G., and Panko, B. (2003), Influence of the El Niño Southern Oscillation on fire regimes in the Florida Everglades. *Ecology*, *84*(12), 3124–3130. doi:10.1890/02-0183.

Bradshaw, L. S., J. E. Deeming, R. E. Burgan, and J. D. Cohen (1984), The 1978 NFDRS: Technical documentation. USDA Forest Service, Report No. Gen Tech Rep INT-169, 44 (U.S. Department of Agriculture, Forest Service, Intermountain Forest and Range Experiment Station, Missoula, MT, USA, 1983).

Brenner, J. (1991), Southern Oscillation anomalies and their relationship to wildfire activity in Florida, *Int. J. Wildland Fire*, *1*(1), 73, doi:10.1071/wf9910073.

Brown, T. J., B. L. Hall, and A. L. Westerling (2004), The impact of twenty-first century climate change on wildland fire danger in the western United States: An applications perspective, *Clim. Change*, *62*(1–3), 365–388, doi:10.1023/b:clim.0000013680.07783.de.

Brown, P. M., E. K. Heyerdahl, S. G. Kitchen, and M. H. Weber (2008), Climate effects on historical fires (1630–1900) in Utah, *Int. J. Wildland Fire*, *17*(1), 28, doi:10.1071/wf07023.

Crimmins, M. A. (2010), Interannual to decadal changes in extreme fire weather event frequencies across the southwestern United States, *Int. J. Climatol.*, *31*, 1573–1583, doi:10.1002/joc.2184.

Eidenshink, J. C., B. Schwind, K. Brewer, Z.-L. Zhu, B. Quayle, and S. M. Howard (2007), A project for monitoring trends in burn severity, *Fire Ecol.*, *3*(1), 321, doi:10.4996/fireecology.0301003.

Fauria, M. M., S. T. Michaletz, and E. A. Johnson (2010), Predicting climate change effects on wildfires requires linking processes across scales. *Wiley Interdiscip. Rev. Clim. Change*, *2*(1), 99–112, doi:10.1002/wcc.92.

Flannigan, M. D., M. A. Krawchuk, W. J. Groot, B. M. Wotton, and L. M. Gowman (2009), Implications of changing climate for global wildland fire, *Int. J. Wildland Fire*, *18*(5), 483, doi:10.1071/wf08187.

Flannigan, M. D., B. M. Wotton, G. A. Marshall, W. J. Groot, J. Johnston, N. Jurko, and A. S. Cantin (2015), Fuel moisture sensitivity to temperature and precipitation: Climate change implications, *Clim. Change*, *134*(1–2), 59–71, doi:10.1007/s10584-015-1521-0.

Fosberg, M. A., J. W. Lancaster, and M. J. Schroeder (1970), Fuel moisture response-drying relationships under standard field conditions, *For. Science*, *16*(1), 121–128.

Garfin, G. M., and B. J. Morehouse (2001), Facilitating use of climate information for wildfire decision-making in the U.S. southwest, in *Fourth Symposium on Fire and Forest Meteorology*, pp. 116–122, American Meteorological Society, Reno, Nev.

Gedalof, Z., D. L. Peterson, and N. J. Mantua (2005), Atmospheric, climatic, and ecological controls on extreme wildfire years in the northwestern United States, *Ecol. Appl.*, *15*(1), 154–174, doi:10.1890/03-5116.

Gershunov, A., and T. P. Barnett (1998), ENSO influence on intraseasonal extreme rainfall and temperature frequencies in the contiguous United States: Observations and model results, *J. Clim.*, *11*(7), 1575–1586, doi:10.1175/1520-0442(1998)0112.0.co;2.

Grantz, K., B. Rajagopalan, M. Clark, and E. Zagona (2007), Seasonal shifts in the North American monsoon, *J. Clim.*, *20*(9), 1923–1935, doi:10.1175/JCLI4091.1.

Hamlington, B. D., R. R. Leben, R. S. Nerem, W. Han, and K. Kim (2011), Reconstructing sea level using cyclostationary empirical orthogonal functions, *J. Geophys. Res.*, *116*, C12015, doi:10.1029/2011JC007529.

Hamlington, B. D., P. E. Hamlington, S. G. Collins, S. R. Alexander, and K.-Y. Kim (2015), Effects of climate oscillations on wind resource variability in the United States, *Geophys. Res. Lett.*, *42*, 145–152, doi:10.1002/2014GL062370.

Hessl, A. E., D. Mckenzie, and R. Schellhaas (2004), Drought and Pacific Decadal Oscillation linked to fire occurrence in the inland Pacific Northwest, *Ecol. Appl.*, *14*(2), 425–442, doi:10.1890/03-5019.

Heyerdahl, E. K., D. McKenzie, L. D. Daniels, A. E. Hessl, J. S. Littell, and N. J. Mantua (2008), Climate drivers of regionally synchronous fires in the inland northwest (1651–1900), *Int. J. Wildland Fire*, *17*, 40–49.

Holden, Z. A., P. Morgan, M. A. Crimmins, R. K. Steinhorst, and A. M. Smith (2007), Fire season precipitation variability influences fire extent and severity in a large southwestern wilderness area, United States, *Geophys. Res. Lett.*, *34*, L16708, doi:10.1029/2007GL030804.

Jolly, W. M., M. A. Cochrane, P. H. Freeborn, Z. A. Holden, T. J. Brown, G. J. Williamson, and D. M. J. S. Bowman (2015), Climate-induced variations in global wildfire danger from 1979 to 2013, *Nat. Commun.*, *6*, 7537, doi:10.1038/ncomms8537.

Kim, K.-Y., B. D. Hamlington, and H. Na (2015), Theoretical foundation of cyclostationary EOF analysis for geophysical and climatic variables: Concepts and examples, *Earth Sci. Rev.*, *150*, 201–18.

Kitzberger, T., P. M. Brown, E. K. Heyerdahl, T. W. Swetnam, and T. T. Veblen (2007), Contingent Pacific–Atlantic Ocean influence on multicentury wildfire synchrony over western North America, *Proc. Natl. Acad. Sci. U.S.A.*, *104*, 543–548.

McKenzie, D., Z. Gedalof, D. L. Peterson, and P. Mote (2004), Climatic change, wildfire, and conservation, *Conserv. Biol.*, *18*, 890–902, doi:10.1111/j.1523-1739.2004.00492.x.

Mesinger, F., et al. (2006), North American regional reanalysis, *Bull. Am. Meteorol. Soc.*, doi:10.1175/BAMS-87-3-342.

Morgan, P., E. K. Heyerdahl, and C. E. Gibson (2008), Multi-season climate synchronized forest fires throughout the 20th century, Northern Rockies, USA, *Ecology*, *89*, 717–728.

Page, Y. L., J. M. Pereira, R. Trigo, C. D. Camara, D. Oom, and B. Mota (2008), Global fire activity patterns (1996–2006) and climatic influence: An analysis using the World Fire Atlas, *Atmos. Chem. Phys.*, *8*(7), 1911–1924, doi:10.5194/acp-8-1911-2008.

Preisler, H. K., D. R. Brillinger, R. E. Burgan, and J. W. Benoit (2004), Probability based models for estimating wildfire risk, *Int. J. Wildland Fire*, *13*, 133–142.

Qian, C., C. Fu, and Z. Wu (2011), Changes in the amplitude of the temperature annual cycle in China and their implication for climate change research, *J. Clim.*, *24*(20), 5292–5302, doi:10.1175/jcli-d-11-00006.1.

Riaño, D., J. A. Ruiz, D. Isidoro, and S. L. Ustin (2007), Global spatial patterns and temporal trends of burned area between 1981 and 2000 using NOAA-NASA Pathfinder, *Global Change Biol.*, *13*(1), 40–50, doi:10.1111/j.1365-2486.2006.01268.x.

Ropelewski, C. F., and M. S. Halpert (1986), North American precipitation and temperature patterns associated with the El Niño/Southern Oscillation (ENSO), *Mon. Weather Rev.*, *114*(12), 2352–2362, doi:10.1175/1520-0493(1986)1142.0.co;2.

Ropelewski, C. F., and M. S. Halpert (1987), Global and regional scale precipitation patterns associated with the El Niño/Southern Oscillation, *Mon. Weather Rev.*, *115*(8), 1606–1626, doi:10.1175/1520-0493(1987)1152.0.co;2.

Swetnam, T. W., and J. L. Betancourt (1990), Fire-southern oscillation relations in the southwestern United States, *Science*, *249*(4972), 1017–1020, doi:10.1126/science.249.4972.1017.

Trouet V., A. H. Taylor, A. M. Carleton, and C. N. Skinner (2006), Fire-climate interactions in forests of the American Pacific coast, *Geophys. Res. Lett.*, *33*, L18704, doi:10.1029/2006GL027502.

Westerling, A. L., H. G. Hidalgo, D. R. Cayan, and T. W. Swetnam (2006), Warming and earlier spring increase western U.S. forest wildfire activity, *Science*, *313*, 940–943.

Williams, A. P., and J. T. Abatzoglou (2016), Recent advances and remaining uncertainties in resolving past and future climate effects on global fire activity, *Curr. Clim. Change Rep.*, *2*(1), 1–14, doi:10.1007/s40641-016-0031-0.

Wolter, K., and M. S. Timlin (2011), El Niño/Southern Oscillation behavior since 1871 as diagnosed in an extended multivariate ENSO index (MEI.ext), *Int. J. Climatol.*, *31*, 1074–1087.

Wu, Z., E. K. Schneider, B. P. Kirtman, E. S. Sarachik, N. E. Huang, and C. J. Tucker (2008), The modulated annual cycle: An alternative reference frame for climate anomalies, *Clim Dyn.*, *31*(7–8), 823–841, doi:10.1007/s00382-008-0437-z.